Hindawi
Journal of Spectroscopy
Volume 2022, Article ID 7238044, 18 pages
https://doi.org/10.1155/2022/7238044

Research Article

Quantitative Raman Spectroscopic Determination of the Composition, Pressure, and Density of CO_2-CH_4 Gas Mixtures

Ying Chen [1,2,3] **and I-Ming Chou** [2]

[1]*CAS Key Laboratory of Mineralogy and Metallogeny and Guangdong Provincial Key Laboratory of Mineral Physics and Materials, Guangzhou Institute of Geochemistry, Chinese Academy of Sciences, Guangzhou 510640, China*
[2]*CAS Key Laboratory of Experimental Study under Deep-sea Extreme Conditions, Institute of Deep-sea Science and Engineering, Chinese Academy of Sciences, Sanya 572000, China*
[3]*University of Chinese Academy of Sciences, Beijing 100049, China*

Correspondence should be addressed to I-Ming Chou; imchou@sidsse.ac.cn

Received 25 April 2022; Accepted 13 August 2022; Published 30 September 2022

Academic Editor: Sarfaraz Ahmed Mahesar

The Raman spectra for pure CO_2 and CH_4 gases and their ten gas mixtures were collected at pressures and temperatures ranging from 2 MPa to 40 MPa and room temperature (~24°C) to 300°C, respectively. A systematic analysis was carried out to establish a methodology for the quantitative determination of the composition, pressure, and density of CO_2-CH_4 mixtures. The shift in the peak position of the υ_1 band for CH_4 was sufficiently large to enable the accurate determination of the pressure of pure CH_4 and CH_4-dominated fluids (>50 mol% CH_4). An equation representing the observed relationship of the peak position of the υ_1 band of CH_4, density, and composition was developed to calculate the density of CO_2-CH_4 mixtures. The Raman quantification factor $F(CH_4)/F(CO_2)$ was demonstrated to be near a constant value of 5.048 ± 0.4 and was used to determine the CH_4 to CO_2 molar ratio in an unknown CO_2-CH_4-bearing fluid with high internal pressure (>10 MPa) based on the Raman peak area ratio. The effect of temperature on the variation in Raman spectral parameters was also investigated at temperatures up to 300°C. The results showed that the effect of temperature must be considered when Raman spectral parameters are used to calculate the pressure, density, and composition of CO_2-CH_4 gas mixtures. Raman spectroscopic analysis results obtained for six samples prepared in fused silica capillary capsules were validated by comparison with the results obtained from microthermometry measurements.

1. Introduction

Carbon dioxide and methane are two important gaseous components in many geological environments and play important roles during geological processes, such as metamorphic reactions, melting, and deformation [1]. CO_2-rich fluid inclusions (FIs) are often found in metamorphic and mantle-derived rocks [2], and occur in close association with many ore deposits [3], such as gold [4], copper [5], and rare Earth element (REE) deposits [6], while CH_4-rich FIs are commonly found in sedimentary basins [7, 8], low-grade metamorphic rocks [9], and mid-ocean ridge hydrothermal environments [10, 11]. However, water-free FIs that are approximated by the CO_2-CH_4 system are common in some metamorphic terranes [12–14]. The information acquired from the composition and density (pressure) of these FIs can be used to help reconstruct the physicochemical conditions under which they and their host minerals are formed [15].

Although several analytical techniques can be used to analyze FIs, only microthermometry (MT) and Raman spectroscopy can provide information on both the composition and pressure of individual inclusions [16, 17]. MT is a nondestructive method based on the observation of phase-transition temperatures. When the melting temperature T_m and homogenization temperature T_h are known, the VX (molar volume and composition) properties can be directly acquired from the VX diagram [18, 19]. However, the uncertainties in the composition and density obtained from the

VX diagram due to the error in T_m and T_h (~±0.1°C) can reach up to ±5 mol% and ±0.09 g·cm^{-3}, respectively [19, 20]. In addition, the microthermometry technique is difficult to apply to small FIs with diameter of <5 μm, low density, and more complex composition [20]. As an alternative to microthermometric measurements, Raman spectroscopy is an extreme useful tool to get quantitative analysis in individual inclusions, partly because it is fast, nondestructive, and high spatial resolution (~1 μm).

Over the past decades, previous studies have been paid more attention to the quantitative analysis of FIs with Raman spectroscopy. Spectral parameters (peak position, peak width, and peak intensity ratio) could be used to determine the pressure, density, and composition of the fluid in FIs. For instance, the concentration of dissolved CH_4 or CO_2 in water solution has been determined based on their peak area (or height) ratio [21–25], and the pressure (or density) of CH_4 can be determined by the peak position of the v_1 band of CH_4 [17, 26–33]. In addition, the CO_2 density in FIs can be obtained by the measurements of the Fermi diad splitting of CO_2 [3, 19, 20, 33–42]. The effect of composition on the Raman spectral parameters of CO_2 and CH_4 was reported earlier by Seitz et al. [17] with low spectral resolution (~5 cm^{-1}) [20]. Recently, calibration data for CO_2-CH_4 mixture and N_2-CO_2-CH_4 mixture have been provided by Le et al. [20] and Sublett et al. [43], respectively. The quantitative relationship between fluid properties (compositions, density, or pressure) and Raman spectral parameters (peak area ratio, peak position, etc.) has to be calibrated carefully with standard samples, since an accurate calibration is fundamental for quantitative measurements.

For two Raman-active species, a and b, in a homogeneous phase, their molar ratios can be calculated from their peak areas [44] based on the following equations:

$$\frac{A_a}{A_b} = \left(\frac{C_a}{C_b}\right) \times \left(\frac{\sigma_a}{\sigma_b}\right) \times \left(\frac{\eta_a}{\eta_b}\right) = \left(\frac{C_a}{C_b}\right) \times \left(\frac{F_a}{F_b}\right), \quad (1)$$

where A is the peak area; C is the concentration; σ is the Raman scattering coefficient; η is the instrumental efficiency factor; and F is the Raman quantification factor [44].

Normally, the reported Raman quantification factors for gaseous are relative to N_2 [45]. However, the reported values for F (CH_4) and F (CO_2) among different laboratories are quite different [19, 20, 38, 46]. Considering that two separate experiments are required to obtain F (CH_4) and F (CO_2), a more practical method is to determine the F (CH_4)/F (CO_2) ratio; then, the molar ratio of CH_4 to CO_2 can be obtained directly according to the peak area ratio A (CH_4)/A (CO_2). In addition, there are only a few Raman spectroscopy calibration data available in the literature for CO_2-CH_4 mixtures at high temperatures up to 300°C, except for the pure CO_2 and CH_4 system [30, 33, 37] and N_2-CO_2-CH_4 system [43].

In this study, an in situ Raman spectroscopy system combined with a fused silica capillary-high-pressure optical cell (FSC-HPOC) is applied to collect Raman spectra for pure CO_2 and CH_4 gases and their CO_2-CH_4 binary mixtures at temperatures ranging from room temperature (~24°C) to 300°C and pressures up to 40 MPa. The peak position and peak area of the v_1 band of CH_4 and the v_1 and $2v_2$ bands (Fermi diad) of CO_2 are systematically analyzed to establish a methodology for the quantitative determination of the composition, pressure, and density of CO_2-CH_4 FIs. The purpose of our work is to construct relationships between Raman spectral parameters and composition, pressure, and density with potential applications to the quantitative study of natural CO_2-CH_4 inclusions. In addition, the effects of temperature on Raman spectral parameters are also investigated. Six synthetic CO_2-CH_4 FIs, prepared in fused silica capillary capsules (FSCCs), were used to perform both laser Raman and MT studies to validate our established methodology.

2. Materials and Methods

2.1. High-Pressure Optical Cell. The instruments and procedures are similar to those used in the study of Lu et al. [29] (Figure 1). The experiments were carried out with a capillary high-pressure optical cell (HPOC [47]). Pure CO_2 and CH_4 gases (99.99%, Jiateng Air Production Inc.) and their ten gaseous mixtures with given compositions (10, 20, 30, 40, 50, 60, 70, 80, 85, and 90 mol% CH_4) were investigated systematically. The HPOC was composed of a fused silica capillary with a circular section (Polymicro Technologies, LLC) with an inner (ID) and outer (OD) diameter of 300 μm and 665 μm, respectively, and a length of approximately 25 cm. The gas or gas mixture was loaded into the HPOC and sealed with a column of mercury (~15 mm long) at one atmospheric pressure. The procedure used for the preparation of the gas samples was described previously in detail [48]. The sample temperature was controlled using a Linkam CAP500 heating-cooling stage. The pressure in the cell was maintained by a water medium in the pressure line and was adjusted using a pressure generator (HiP Model no. 37-6-30). The pressure was read using a Setra 204D digital pressure transducer with a Datum 2000™ manometer (69 MPa full scale, accurate to ±0.14% of full scale).

2.2. Fused Silica Capillary Capsule. Fused silica capillary capsules (FSCCs; 300 μm OD, 100 μm ID, and approximately 1.0 cm long) were constructed to contain the CO_2-CH_4 mixture gas using the sample-loading system of Chou et al. [47], and they were used for verification of our quantitative Raman spectroscopic analyses of the CO_2-CH_4 system. First, the line was flushed twice with one gas (CH_4 or CO_2) after placing under vacuum. Then, gas at a pressure of slightly lower than 0.2 MPa was loaded into the line and silica tube, and the closed end of the tube was immersed in liquid nitrogen to form liquid or solid CH_4/CO_2. Second, the system was evacuated, while the closed end was still immersed in liquid nitrogen, and the silica tube was then pressurized with another gas (CO_2 or CH_4). Third, the system was evacuated again, and the open end of the tube was sealed with a hydrogen flame in vacuum, while the closed end remained immersed in liquid nitrogen. A higher loading concentration in CO_2-CH_4 mixture was obtained for the gas loaded first. Even though CO_2-CH_4 gas mixtures

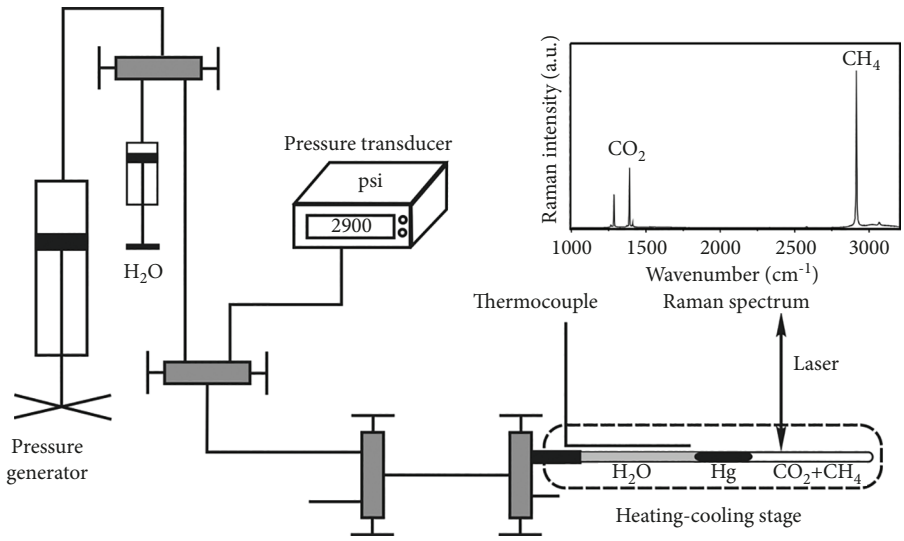

Figure 1: Schematic diagram of the experimental system (modified after Lu et al. [29]).

with known proportions could also be loaded directly into the FSC tubes, we found that their proportions changed slightly due to the different freezing temperature while freezing.

2.3. Microthermometry Analyses of FSCC Samples. Microthermometric analyses of the FSCC samples were carried out using a Linkam CAP500 heating-cooling stage under the Olympus microscope in the laser Raman spectroscopic system. The temperature was calibrated with the triple points of H_2O (±0°C) and CO_2 (−56.6°C) and was accurate to ±0.1°C. In the present study, measurements of the phase changes were carried out only below room temperature. The system was cooled rapidly at a rate of 10°C/min to −180°C, and after holding for 10 minutes, it was then heated at a rate of 10°C/min. The heating rate was reduced to 0.3°C/min at a temperature of approximately 5°C below the phase transition point to precisely determine the temperature of the phase changes. The same rates were used for heating-cooling cycling. The CO_2-CH_4 system shows three phases at low temperatures: solid CO_2, liquid, and vapor. Two phase transition temperatures can be measured during heating from −180°C to room temperature: the final melting temperature of solid CO_2 (T_m) and the L-V homogenization temperature (T_h) for the disappearance of the liquid phase or vapor bubble [49]. The measured values for T_m and T_h were then used to calculate the composition and density of the FSCC samples based on the *VX* diagram of Thiery et al. [18].

2.4. Collection and Calibration of Raman Spectra. Raman spectra were acquired using a JY/Horiba LabRam HR Evolution Raman system equipped with a 532.06 nm (frequency-doubled Nd: YAG) laser, an SLWD 50× Olympus objective with a numerical aperture of 0.35, and an 1800 groove/mm grating with a spectral resolution of approximately 0.65 cm^{-1} or a 600 groove/mm grating with a spectral resolution of approximately 2 cm^{-1}. Approximately 20 mW of laser light was focused onto the center of the horizontal tube to generate Raman signals during the measurement.

Raman spectra for CO_2 and CH_4 are shown in Figure 2. CO_2 has five Raman bands, including the Fermi diad of CO_2 between 1200 and 1400 cm^{-1} (the lower band at ~1285 cm^{-1} and the upper band at ~1388 cm^{-1}), two hot bands flanking the Fermi diad at ~1265 and 1409 cm^{-1}, and a weak CO_2 band at 1370.0 cm^{-1} due to the isotopic splitting of $^{13}CO_2$ [37]. CH_4 has four Raman bands: the asymmetric bending overtone band ($2\upsilon_4$ at ~2580 cm^{-1}), the C-H symmetric stretching band (υ_1 at ~2917 cm^{-1}), the asymmetric stretching band (υ_3 at ~3020 cm^{-1}), and the asymmetric bending overtone band ($2\upsilon_2$ at ~3070 cm^{-1}) [50]; the other three bands have an intensity that is ~2% of that of the υ_1 band. In this study, only the Fermi diad and hot bands of CO_2 and υ_1 band of CH_4 (approximately 2917 cm^{-1}) were investigated.

As shown in Figure 2, the 600 groove/mm grating, with a lower spectral resolution but wider spectral range, was used for collecting spectra in multiple windows ranging between 1000 cm^{-1} and 3200 cm^{-1} to cover the peaks of the Fermi diad of CO_2 and CH_4. In addition, spectra employing the 1800 groove/mm grating with a high spectral resolution were also collected in two single windows to obtain precise peak positions. One window ranged between 1170 cm^{-1} and 1620 cm^{-1}, which covers the Fermi diad of CO_2 (1200~1400 cm^{-1}), and two well-established reference peaks of benzonitrile (1192.6 and 1598.9 cm^{-1}) was used to calibrate the Fermi diad of CO_2. The other window ranged between 2718 cm^{-1} and 3075 cm^{-1}, which covers the CH_4 peak at approximately 2917 cm^{-1}; neon lines at 626.649 nm (2836.976 cm^{-1}) and 630.479 nm (2933.916 cm^{-1}) were selected to calibrate the peak position of CH_4 [30].

The measured spectra with single windows for CO_2 and CH_4 were fitted with the program PeakFit v4.12 (AISN Software Inc.) using Gaussian–Lorentzian functions without smoothing or baseline correction before peak-fitting procedures. The real peak positions of CO_2 and CH_4 were derived from the following relations:

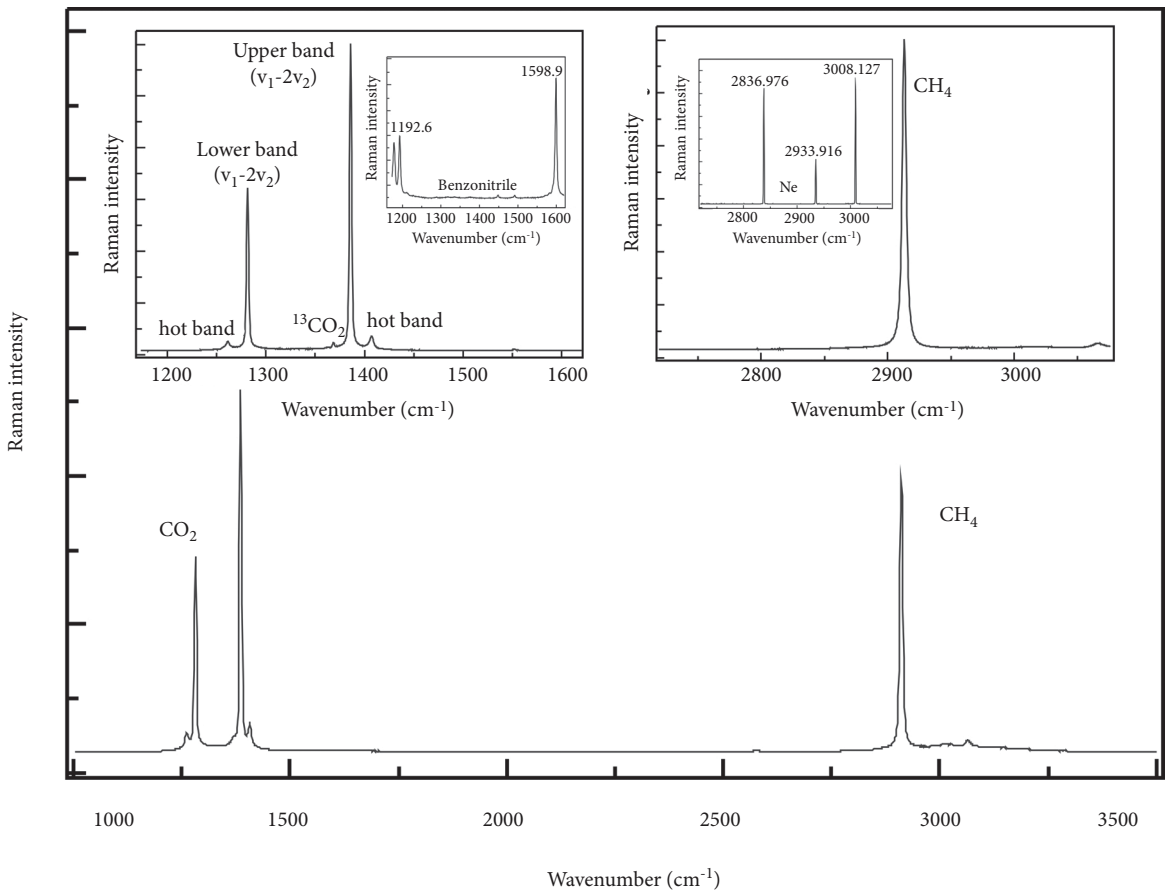

FIGURE 2: Raman spectrum of the CO_2-CH_4 mixture showing the Raman lines for CO_2 and CH_4. The top left insert shows the detailed spectrum of CO_2 containing Fermi diad bands, two hot bands, $^{13}CO_2$, and the spectrum for benzonitrile. The two marked peaks for benzonitrile (1192.6 and 1598.9 cm^{-1}) were used to calibrate the CO_2 Fermi diad splitting. The right insert shows the C-H symmetric v_1 band of CH_4 and Ne emission lines at 2836.976 cm^{-1}, 2933.916 cm^{-1}, and 3008.127 cm^{-1}. The Ne emission lines at 2836.976 cm^{-1} and 2933.916 cm^{-1} bracket the v_1 band of CH_4 and were used to calibrate the CH_4v_1 peak position.

$$\frac{v_{\text{real}} - 1192.6}{v_m - \text{Benz}_{m1}} = \frac{1598.9 - 1192.6}{\text{Benz}_{m2} - \text{Benz}_{m1}}, \quad (2)$$

$$\frac{v_{\text{real}} - 2836.976}{v_m - \text{Ne}_{m1}} = \frac{2933.916 - 2836.976}{\text{Ne}_{m2} - \text{Ne}_{m1}}, \quad (3)$$

where υ_{real} is the real position of the upper and lower bands of the Fermi diad of CO_2 in equation (2) and the C-H symmetric stretching band (v_1) of CH_4 in equation (3); υ_m is the measured peak position of CO_2 or CH_4; Benz_{m1} and Benz_{m2} are the two reference peaks of benzonitrile; and Ne_{m1} and Ne_{m2} are the measured wavenumbers of the two reference neon lines.

The Raman peak area ratio (PAR) of the upper band of the Fermi diad of CO_2 to the C-H symmetric stretching band (v_1) of CH_4 was determined by the software GRAMS/AI (Thermo Galactic). Three spectra were collected at each set *P-T* condition.

3. Results and Discussion

3.1. Determination of the Pressure of the CO_2-CH_4 Gas Mixtures. The calibrated peak positions for the CH_4v_1 peak and the lower and upper members of the CO_2 Fermi diad and the Fermi diad splittings for all samples at room temperature and various pressures collected in HPOC are listed in Table S1 and S2 (Supplemental material) and shown in Figure 3. Figure 3(a) shows the peak positions for the v_1 peak of CH_4 in pure CH_4 and ten CO_2-CH_4 mixtures as a function of total pressure; the addition of CO_2 can affect the peak position of CH_4; however, the dominant factor affecting the peak position of CH_4 is the total fluid pressure, which is in agreement with the result of Seitz et al. [17]. A leap in v_1 peak position for CH_4 in Figure 3(a) is evident for CO_2-rich mixtures at low pressure. For the 10 mol% CH_4-90 mol% CO_2 mixture, this abrupt shift in the peak position in response to pressure represents the liquid-vapor phase transition. The 30% CH_4-70% CO_2 mixture, however, remains supercritical (but near-critical) at room temperature [17].

The lower and upper members of the Fermi diad peaks for CO_2 and Fermi diad splitting for CO_2 in CO_2-CH_4 mixtures as a function of pressure are presented in Figures 3(b)–3(d), respectively. The peak shift with pressure from 2 MPa to 40 MPa is much greater for the lower Fermi diad member (~5 cm^{-1}) than for the upper Fermi diad

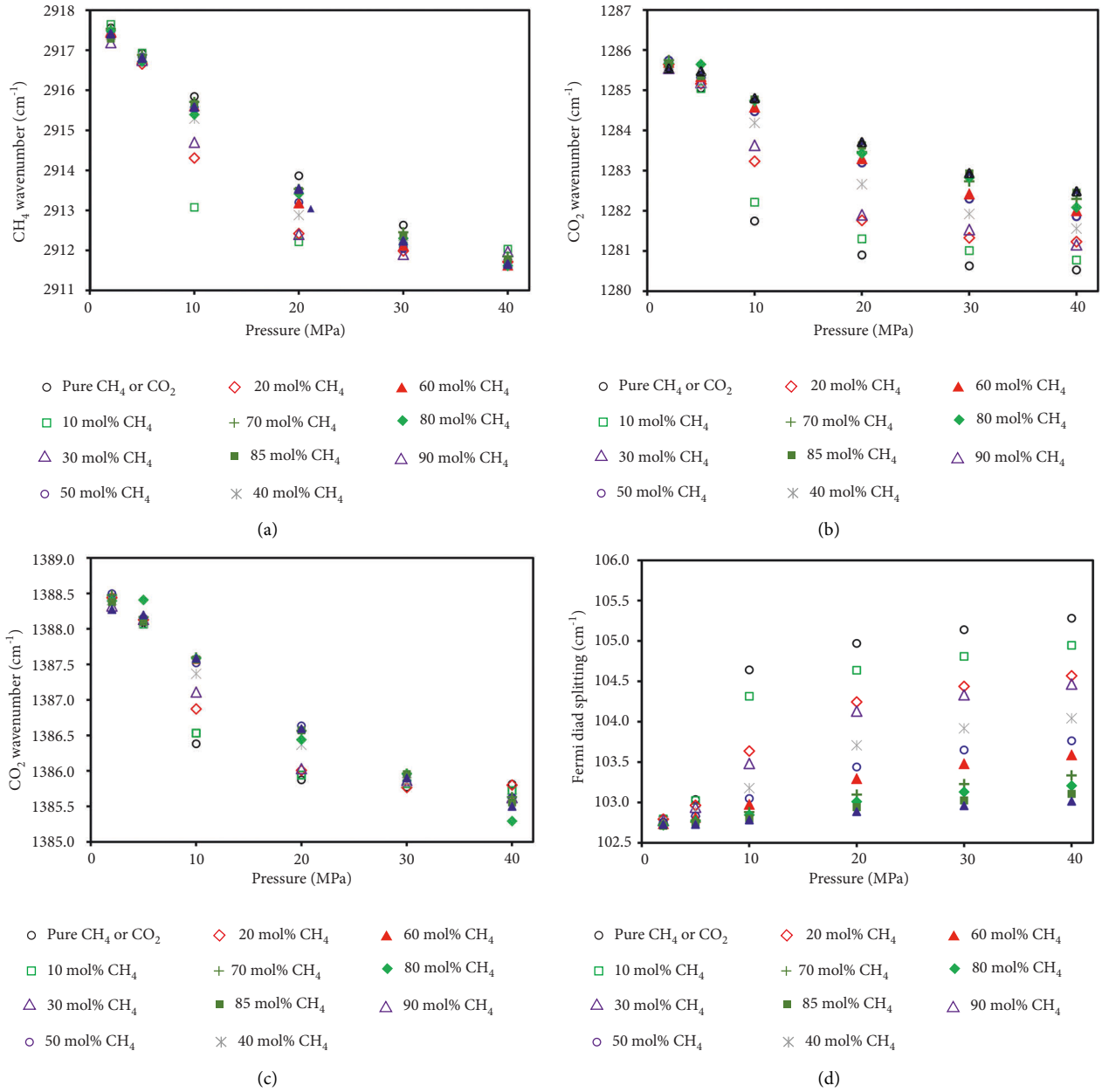

FIGURE 3: Raman peak positions for the $CH_4 v_1$ peak (a) and the lower (b) and upper (c) members of the CO_2 Fermi diad and the Fermi diad splitting (d) for different CO_2-CH_4 gaseous mixtures at room temperature as a function of pressure.

member (~3 cm^{-1}). Thus, the peak position of the lower Fermi diad member is a more sensitive monitor of fluid pressure, which are consistent with previous studies [41]. However, the peak position of the lower Fermi diad member is also more sensitive to composition. Indeed, the Fermi diad splitting (Δ, the separation between bands in the Fermi diad) of CO_2 has been previously used to determine the pressure or density of CO_2 in FIs [37, 40]. Our results show that at 2 MPa, Δ is nearly identical (~102.76 cm^{-1}) for any composition, while at higher pressures, the effect of the gas mixture composition becomes more obvious, which is similar to that observed for CO_2 mixed with N_2 and CH_4 [19, 20]. Therefore, we can draw the same conclusion with previous studies [17, 20] that the Δ for CO_2 is not only a function of pressure but also a function of the composition of the CO_2-CH_4 gas mixture (Figure 3(d)).

As mentioned above, it can be concluded that the $CH_4 v_1$ peak could be the most suitable parameter for the pressure determination, although there is an abrupt shift in the CH_4 peak positions due to the existence of the liquid-vapor transition in CO_2-rich mixtures. As shown in Figure 4, different laboratories have their own calibration curves for the CH_4 peak position-pressure relationship. It can be ascribed to different measurement conditions, including excitation wavelength, the numerical aperture of the objective, the slit width, and the groove density of grating. However, all

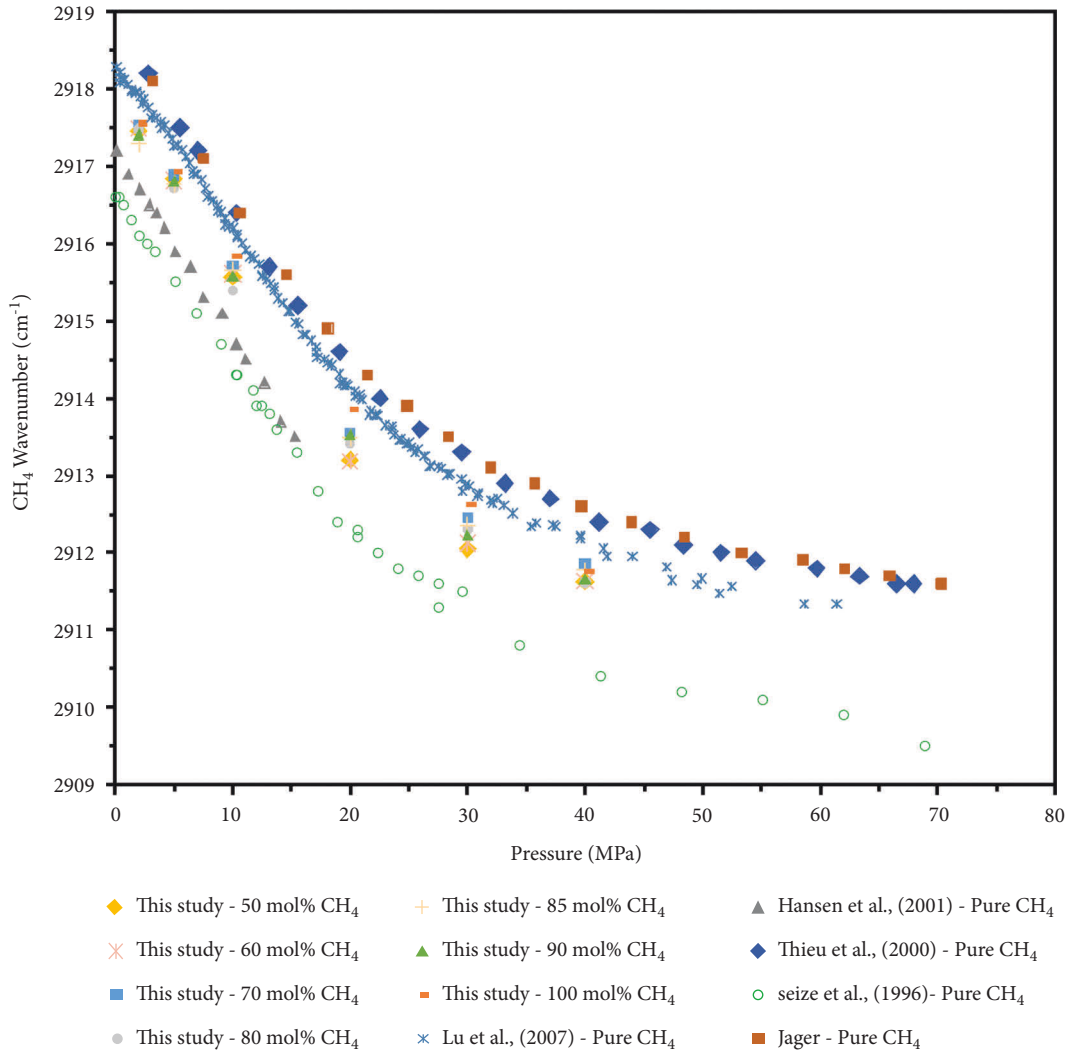

Figure 4: Raman peak position of C-H symmetric stretching band (υ_1) of CH_4 from six available data sets as a function of pressure.

six data sets collected from the literature for pure CH_4 and from this study for CH_4-rich mixture have similar relations between peak position and pressure, which are almost parallel to each other but with different intercepts at zero pressure, indicating that systematic discrepancies may exist among these data sets. Fortunately, these discrepancies can be eliminated by choosing D as a variable (Figure 5), where $D = \upsilon_p - \upsilon_0$, the difference between the peak positions at elevated pressure (υ_p) and near-zero pressure (υ_0) (in this study, $\upsilon_0 = 2917.924\ \text{cm}^{-1}$ for <0.1 MPa). The same treatment was successfully demonstrated for pure CH_4 many years ago by Lu et al. [29]. Our data (CH_4-rich mixtures with $CH_4 \geq 50$ mol% and pure CH_4) at room temperature agree with previous studies [17, 27, 29, 51] for pure CH_4 (Figure 5). After fitting the data obtained from the six sources, the relation between D (in cm^{-1}) and pressure P (in MPa) can be described by the following equation:

$$D = 2.6953 \times 10^{-8} P^5 - 5.0314 \times 10^{-6} P^4 + 3.1297 \times 10^{-4} P^3 - 5.1191 \times 10^{-3} P^2 - 1.9752 \times 10^{-1} P, \quad (4)$$

with R^2 (squared correlation coefficient) = 0.9972. The uncertainty (1σ) in the calculated pressure was ±1.1 MPa. This equation could be used to correlate P with D in other laboratories and calculate the pressure (≤70 MPa) of CH_4-rich mixtures ($CH_4 \geq 50$ mol%) with the measured peak position of the $CH_4\upsilon_1$ band near room temperature, as long as υ_0 is known for the particular Raman spectrometer.

3.2. Determination of the Density of CO_2-CH_4 Gas Mixtures. The pressure of the CO_2-CH_4 gas mixtures of known composition at room temperature (~24°C) was converted to density using the GERG-2008 EoS (equation of state), which is a new wide-range EoS for natural gases and other mixtures of 21 natural gas components [52]. The variations in D and Δ within CO_2-CH_4 gas mixtures as a function of density and composition are plotted in Figure 6. The results show that D decreases with increasing CH_4 concentration and density of the gas mixture, whereas Δ increases with elevated CO_2 concentration and density. The maximum value of the variation in Δ is quite small (<~3 cm^{-1}) compared to that for

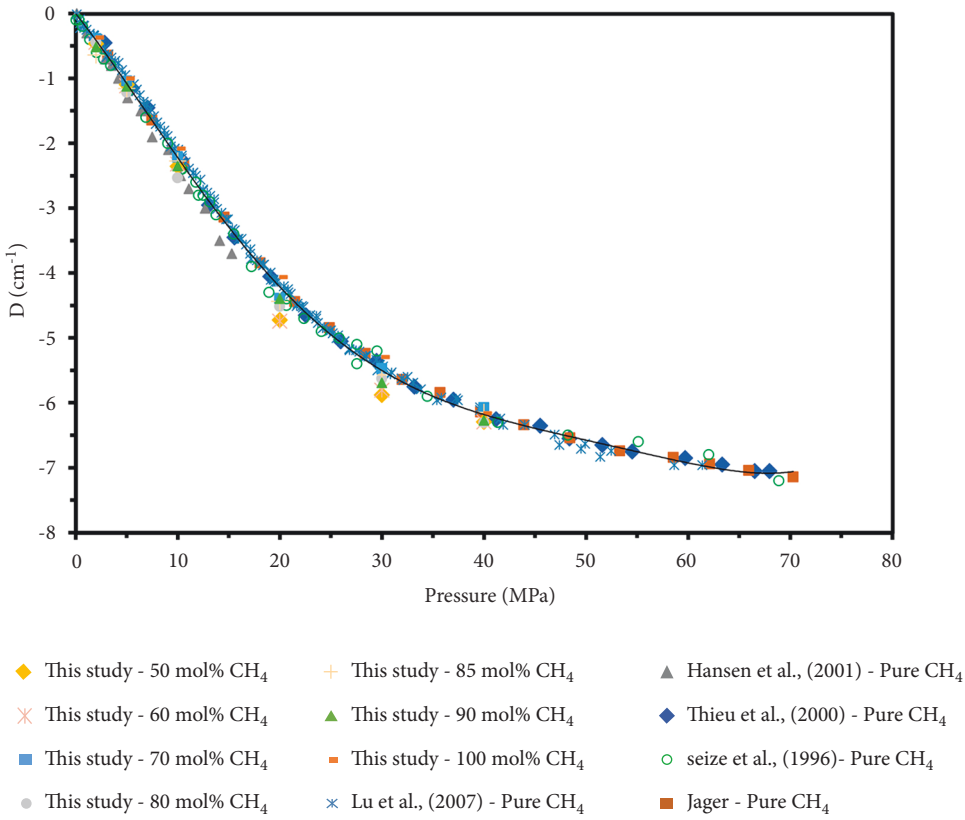

Figure 5: The P-D relationship determined in this study compared with other published values at near room temperature. Note that the original data of Jager's Colorado School of Mines are cited from Lu et al. [29].

D (<~6 cm^{-1}) over the same density range (0~1 g/cm^3). Thus, given an analytical uncertainty of ±0.01 cm^{-1} for the measurement of the peak position, D will generally provide the most precise estimate of density. Therefore, the experimental data for D in CO_2-CH_4 gas mixtures were fitted to the following equation by polynomial regression analysis (using the software 1stOpt):

$$\begin{aligned}\rho = {} & a_{00} + a_{10} \times C_{CH4} + a_{01} \times D + a_{20} \times C_{CH4}^2 \\ & + a_{11} \times C_{CH4} \times D + a_{02} \times D^2 + a_{30} \times C_{CH4}^3 \\ & + a_{21} \times C_{CH4}^2 \times D + a_{12} \times C_{CH4} \times D^2 + a_{03} \times D^3 \\ & + a_{31} \times C_{CH4}^3 \times D + a_{22} \times C_{CH4}^2 \times D^2 \\ & + a_{13} \times C_{CH4} \times D^3 + a_{04} \times D^4.\end{aligned} \quad (5)$$

The fitted coefficients for equation (5) are listed in Table 1, and the root-mean-square error of equation (5) is 0.012 g/cm^3 with an R^2 of 0.997. This equation can be used to calculate the density of CH_4-CO_2 mixtures with the measured peak position of the $CH_4 v_1$ band near room temperature.

3.3. Determination of F (CH_4)/F (CO_2). The ratio of the peak areas of the v_1 band of CH_4 and the upper Fermi diad member of CO_2 (A (CH_4)/A (CO_2)) for CO_2-CH_4 mixtures increases with pressure below 10 MPa and then maintains the same levels at higher pressures (Table 2), indicating that it is an advantageous to use the ratios of the peak area of the v_1 band of CH_4 and the upper Fermi diad member of CO_2 for quantitative determinations of the fluid composition in CO_2-CH_4 mixtures [17].

According to equation (1), if F (CH_4)/F (CO_2) has been determined by the known A (CH_4)/A (CO_2) and C (CH_4)/C (CO_2), then it can be used to determine the molar ratio of CH_4 to CO_2 in an unknown CO_2-CH_4-bearing fluid from the Raman peak area ratio. F (CH_4)/F (CO_2) in ten CO_2-CH_4 gaseous mixtures were calculated based on equation (1) and listed in Table 2. Within a given CO_2-CH_4 gaseous mixture, the F (CH_4)/F (CO_2) value rises at low pressures and remains constant (within analytical uncertainty) above 10 MPa (Table 2), which is in agreement with the previous work of Seitz et al. [17]. Therefore, the F (CH_4)/F (CO_2) values obtained at 20 MPa, 30 MPa, and 40 MPa were averaged and considered as the general F (CH_4)/F (CO_2) value of this mixture. It can be found that the general F (CH_4)/F (CO_2) value varies somewhat with different gaseous mixtures. Figure 7 shows a good linear relationship between the molar ratio (C (CH_4)/C (CO_2)) and peak area ratio (A (CH_4)/A (CO_2)) with an R^2 of 0.9995. The slope shows a value of 5.048, which represents the F (CH_4)/F (CO_2) ratio based on equation (1). The uncertainty in the average values of F (CH_4)/F (CO_2) is ±0.4, which in turn can lead to an average error in the composition up to ±1.4 mol% CH_4.

Table 3 shows a comparison of our results with those obtained in six previous studies. The results show that F

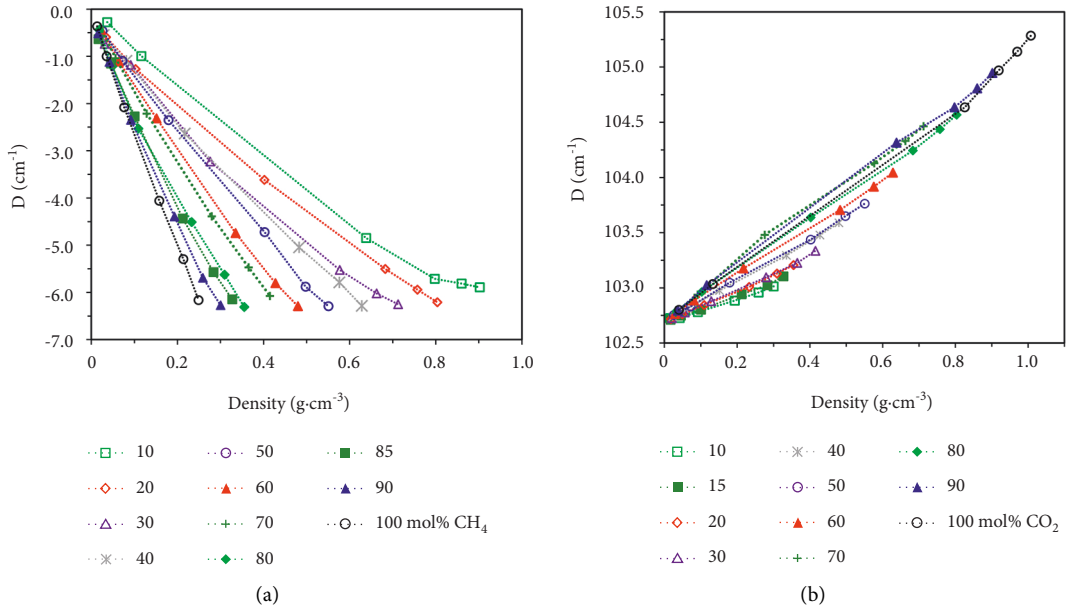

FIGURE 6: The variation in D (a) and Δ (b) within CO_2-CH_4 gas mixtures as a function of density and composition. $D = \upsilon_p - \upsilon_0$ is the difference between the υ_1 peak positions of CH_4 at elevated pressure (υ_p) and near-zero pressure (υ_0); Δ represents the separation between bands in the Fermi diad of CO_2.

TABLE 1: The fitting parameters for equation (5).

a_{00}	0.0458578972
a_{10}	0.0070465891
a_{01}	−0.0367435722
a_{20}	−0.3041825424
a_{11}	−0.0208569183
a_{02}	0.0264438359
a_{30}	0.2888501741
a_{21}	−0.0290891828
a_{12}	−0.0400853154
a_{03}	0.0014973436
a_{31}	0.0879585851
a_{22}	0.0270909951
a_{13}	0.0002772730
a_{04}	0.0000945387

$(CH_4)/F$ (CO_2) is quite different among different laboratories. Our value is in agreement with four previous results [17, 19, 20, 53]. Seitz et al. [17] stated that the variation in $F(CH_4)/F(CO_2)$ is not significant within their analytical uncertainty, and the average value of $F(CH_4)/F(CO_2)$ determined in five different CO_2-CH_4 mixtures at 20 MPa is 5.16 ± 0.18. Le et al. [19, 20] reported the $F(CH_4)$ and $F(CO_2)$ (relative to N_2) to be 7.73 ± 0.16 and 1.40 ± 0.03, respectively, yielding an $F(CH_4)/F(CO_2)$ ratio of 5.52 ± 0.16. They also argued that the difference between different concentrations is not significant for the measured composition of the gas mixtures. Wopenka and Pasteris [44] obtained an average $F(CH_4)/F(CO_2)$ of 4.4 ± 0.15 in a variety of CO_2-CH_4-bearing gas mixtures at low pressure (≤1.6 MPa). Qiu et al. [32] determined a $F(CH_4)$ of 6.420 ± 0.104 and a $F(CO_2)$ of 1.690 ± 0.042 in a CH_4-CO_2-CO-N_2 mixture with a molar ratio of 1 : 1 : 1 : 2 from 10 MPa to 60 MPa, yielding an $F(CH_4)/F(CO_2)$ ratio of 3.80 ± 0.10.

4. Influence of Temperature on the Raman Spectral Parameters

To study the influence of temperature on the Raman spectra measured for CO_2-CH_4 gas mixtures, HPOC was used to collect Raman spectra for five CO_2-CH_4 gas mixtures (10 mol% CH_4, 30 mol% CH_4, 50 mol% CH_4, 70 mol% CH_4, and 90 mol% CH_4) ranging from room temperature to 300°C and from 2 MPa to 40 MPa. The pressures and temperatures of the CO_2-CH_4 gas mixtures of known composition were converted to density using the GERG-2008 EoS.

4.1. Influence of Temperature on the Relationship between Peak Position and Pressure/Density for CO_2-CH_4 Gas Mixtures. The peak positions of the υ_1 band of CH_4 and Fermi diad splitting (Δ) of CO_2 for pure CH_4 or CO_2 gas and their five CO_2-CH_4 gas mixtures at various temperatures and pressures are listed in Table S3 (Supplemental material) and shown in Figures 8 and 9. As shown in Figure 8, as the temperature increases at constant pressure, the peak positions of the υ_1 band of CH_4 and Fermi diad splitting (Δ) of CO_2 for the five CO_2-CH_4 gas mixtures shift to higher and lower wavenumbers, respectively. The results show that the effect of temperature on the peak positions of CH_4 and CO_2 in the mixed system has the same trend as demonstrated previously for the pure CH_4 or CO_2 system [30, 33, 37] and N_2-CO_2-CH_4 system [43]. The pressure-induced change in the shift decreases at higher temperatures (Figure 8). Additionally, at room temperature, there is an abrupt shift in the measured position of CH_4 and CO_2 resulting from the

Table 2: The F (CH_4)/F (CO_2) in ten CO_2-CH_4 gaseous mixtures at room temperature and pressures up to 40 MPa.

P (MPa)	X_{CH4} (mol%)	[a]A (CH_4)/ A (CO_2)	F (CH_4)/ F (CO_2)
2		0.431	3.878
5		0.445	4.006
10		0.449	4.043
20	10	0.453	4.074
30		0.445	4.008
40		0.446	4.010
Avg.		0.448	4.031
2		0.994	3.978
5		1.037	4.147
10		1.078	4.314
20	20	1.055	4.219
30		1.059	4.235
40		1.063	4.250
Avg.		1.059	4.235
2		1.763	4.114
5		1.852	4.322
10		1.890	4.409
20	30	1.930	4.504
30		1.925	4.491
40		1.919	4.477
Avg.		1.925	4.491
2		2.873	4.309
5		2.976	4.463
10		3.021	4.531
20	40	3.021	4.531
30		3.027	4.540
40		3.044	4.565
Avg.		3.030	4.545
2		4.698	4.698
5		4.788	4.788
10		4.928	4.928
20	50	4.836	4.836
30		4.658	4.658
40		4.691	4.691
Avg.		4.728	4.728
2		6.643	4.429
5		6.919	4.613
10		7.072	4.714
20	60	7.165	4.777
30		7.176	4.784
40		7.198	4.799
Avg.		7.180	4.787
2		11.945	5.119
5		12.492	5.354
10		11.974	5.132
20	70	12.928	5.541
30		12.616	5.407
40		12.525	5.368
Avg.		12.690	5.430
2		18.170	4.542
5		18.541	4.635
10		18.808	4.702
20	80	19.427	4.857
30		19.652	4.913
40		19.516	4.879
Avg.		19.531	4.883
2		27.075	4.778
5		28.308	4.996
10		28.129	4.964
20	85	28.781	5.079
30		28.821	5.086
40		28.606	5.048
Avg.		28.736	5.071
2		39.812	4.424
5		41.345	4.594
10		42.173	4.686
20	90	46.208	5.134
30		45.496	5.055
40		44.950	4.994
Avg.		45.551	5.061

[a]A is the Raman peak area.

phase transition, but this shift vanishes at higher temperatures (above 100°C). At the same pressure and temperature, υ_{CH4} and Δ in the gas mixtures are shifted to lower wavenumbers compared with the values in the pure system (Figures 9(a) and 9(b)), which have also been reported in previous studies [17, 20]. However, in the N_2-CO_2-CH_4 system, υ_{CH4} is located at higher wavenumbers relative to the pure system at the same P-T conditions [43]. Figure 10 presents the variation in υ_{CH4} and Δ as a function of density, composition, and temperature. The difference in density is notable at various temperatures. Taking 10 mol% CH_4 at 40 MPa as an example, the density and Raman shift of υ_{CH4} at 24°C are 0.902 g/cm^3 and 2912.03 cm^{-1}, respectively, and at 300°C, they are 0.338 g/cm^3 and 2914.0 cm^{-1}, respectively. In conclusion, the effect of temperature must be considered when Raman shifts are used to calculate the pressure or density of CO_2-CH_4 gas mixtures.

Effect of temperature on the variation of (a) the υ_1 band of CH_4 and (b) Fermi diad splitting of CO_2 (Δ) as a function of the density of CO_2-CH_4 mixtures.

The relationship between the molar ratio and peak area ratio (average values above 10 MPa) is plotted at different temperatures in Figure 12 and listed in Table 4. This indicates that F (CH_4)/F (CO_2) increases with increasing temperature, and the peak area ratio obtained at high temperatures is not suitable for determining the composition at room temperature because it could lead to an overestimation of the molar ratio of CH_4/CO_2. Therefore, the temperature effect must be considered when CH_4 to CO_2 peak area ratios are used to calculate the fluid composition in CO_2-CH_4 mixtures.

4.2. Effect of Temperature on the Raman Peak Area for CO_2-CH_4 Gas Mixtures. The ratios of the peak area of the υ_1 band of CH_4 and the upper Fermi diad of CO_2 for the 50 mol% CH_4-50 mol% CO_2 ($C_{CH4}/C_{CO2} = 1:1$) mixture are plotted at different temperatures as a function of pressure in Figure 11.

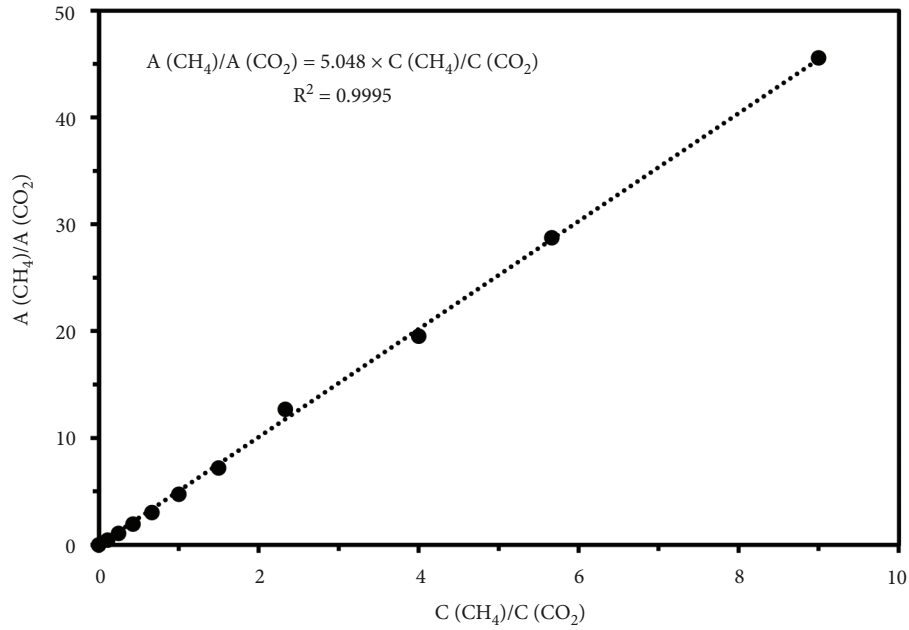

Figure 7: The linear relationship between the molar ratio C (CH_4)/C (CO_2)) and the Raman peak area ratio (A (CH_4)/A (CO_2)) at room temperature.

Table 3: Comparison of F (CH_4)/F (CO_2) in this study with previous works.

	This study	Ref. [17]	Ref. [19, 20]	Ref. [32]	Ref. [44]	Ref. [53]	Ref. [54]
λ (nm)	532.07	514.5	514.5	532	514.5	514.5	514
Pressure (MPa)	2–40	20	0.5–60	1–60	<1.6	0.1	5, 10
Temperature (°C)	24	22	32	22	—	—	22
C (CH_4)/C (CO_2)	0.11~9	0.11~9	0.11~9	1	—	—	0.43~2.33
F (CH_4)/F (CO_2)	5.05 ± 0.4	5.16 ± 0.18	5.52 ± 0.16	3.8 ± 0.1	4.40 ± 0.15	5.05	11.12

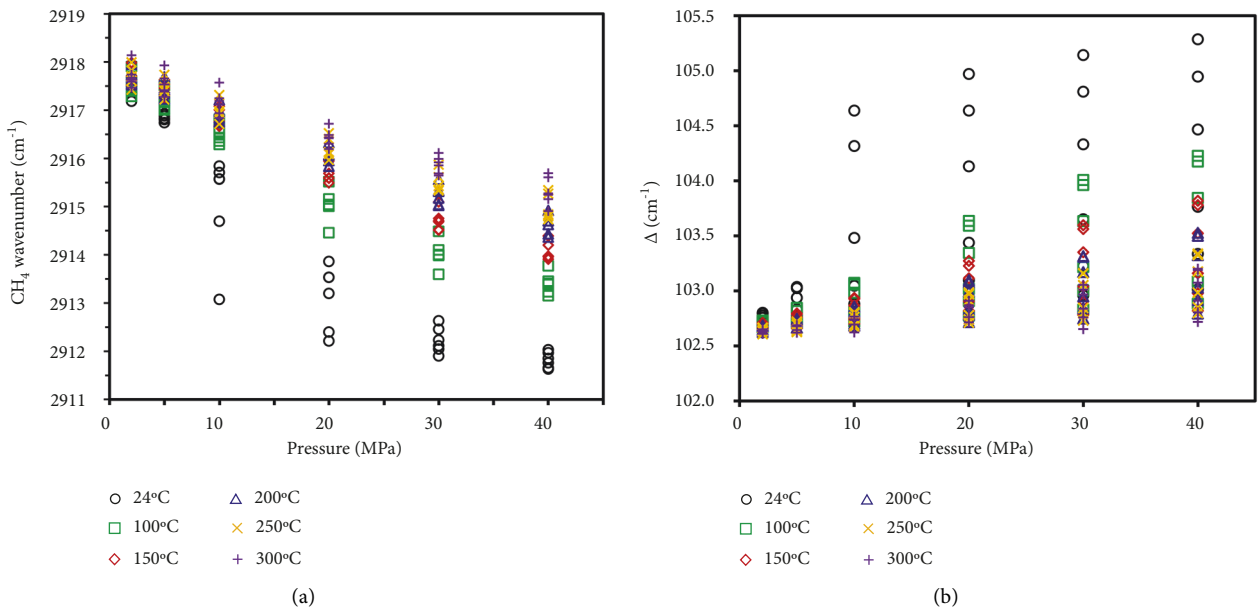

Figure 8: Effect of temperature on the Raman peak positions of (a) the v_1 band of CH_4 and (b) Fermi diad splitting of CO_2 (Δ) for five CO_2-CH_4 gas mixtures as a function of pressure.

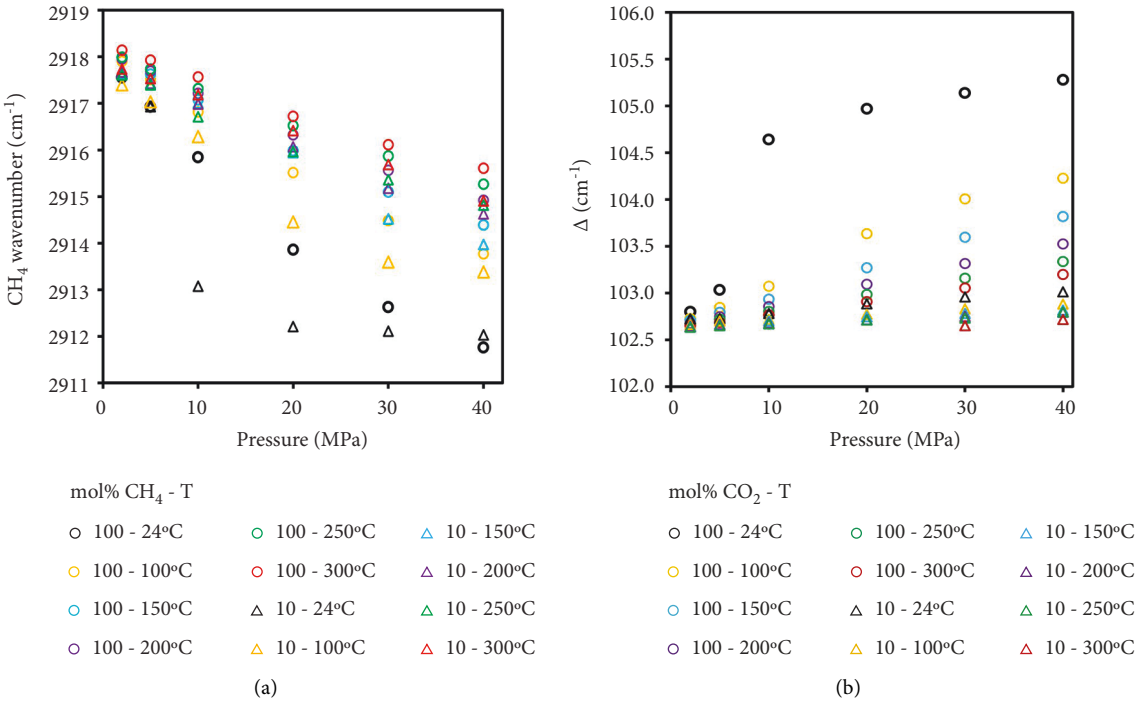

Figure 9: Effect of temperature on the Raman peak positions of (a) the υ_1 band of CH_4 for pure CH_4 and 10 mol% CH_4 and (b) Fermi diad splitting of CO_2 (Δ) for pure CO_2 and 10 mol% CH_4 as a function of pressure.

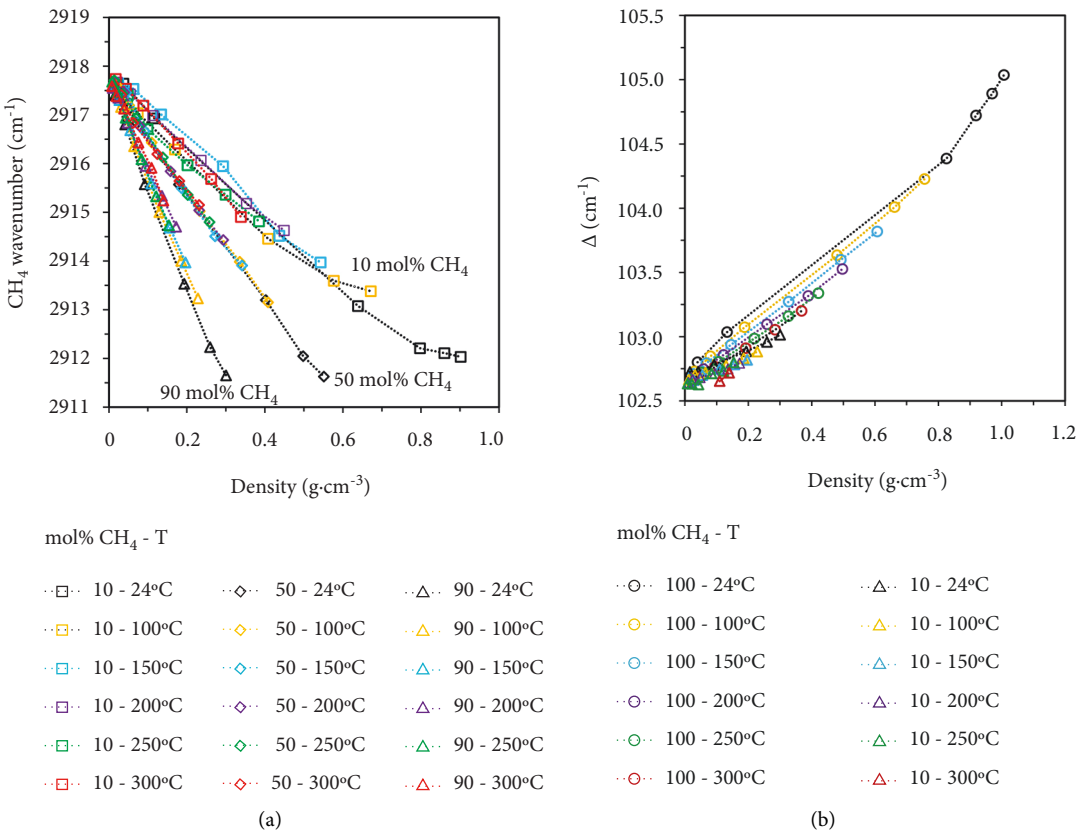

Figure 10: Effect of temperature on the variation of (a) the υ_1 band of CH_4 and (b) Fermi diad splitting of CO_2 (Δ) as a function of the density of CO_2-CH_4 mixtures.

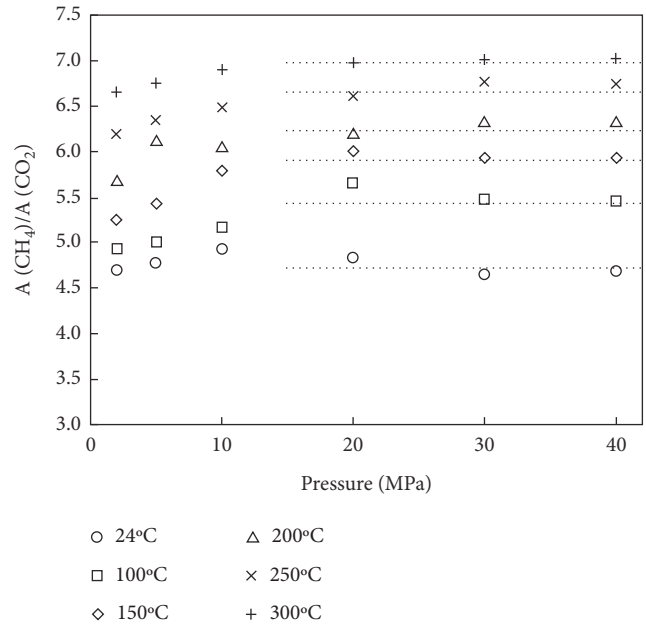

Figure 11: Relationship between the CH_4 to CO_2 peak area ratio and pressure at 50 mol% CH_4-50 mol% CO_2 mixture and temperatures ranging from 24°C to 300°C.

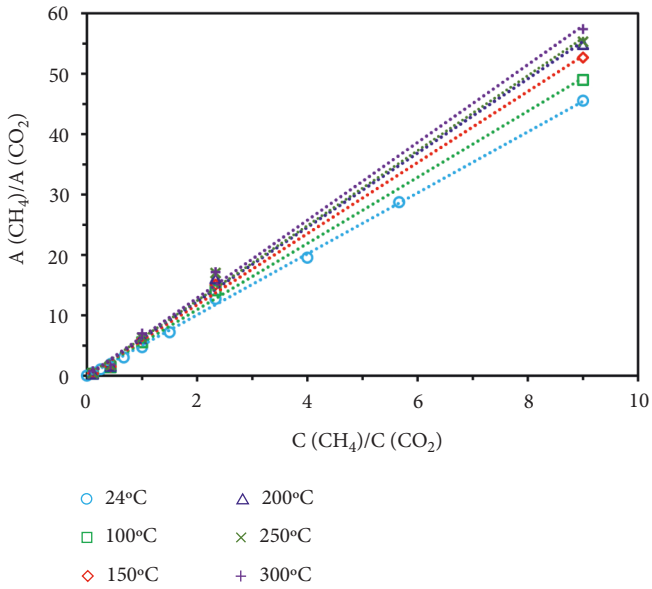

Figure 12: Raman peak area ratio between CH_4 and CO_2 as a function of their molar ratio at different temperatures.

Table 4: The fitting parameters for equation (1) at different temperatures.

Temperature (°C)	24	100	150	200	250	300
F (CH_4)/F (CO_2)	5.048	5.4770	5.8846	6.147	6.2119	6.4383
R^2	0.9995	0.9989	0.9990	0.9987	0.9977	0.9983

The results show that the A (CH_4)/A (CO_2) rises steeply with increasing pressure up to 10 MPa and then becomes approximately constant at higher pressures, ranging from 4.7 at 24°C to 7.0 at 300°C.

4.3. Effect of Temperature on the Hot Band of CO_2 for CO_2-CH_4 Gas Mixtures. Earlier studies have confirmed that the intensity of CO_2 hot bands increases with increasing

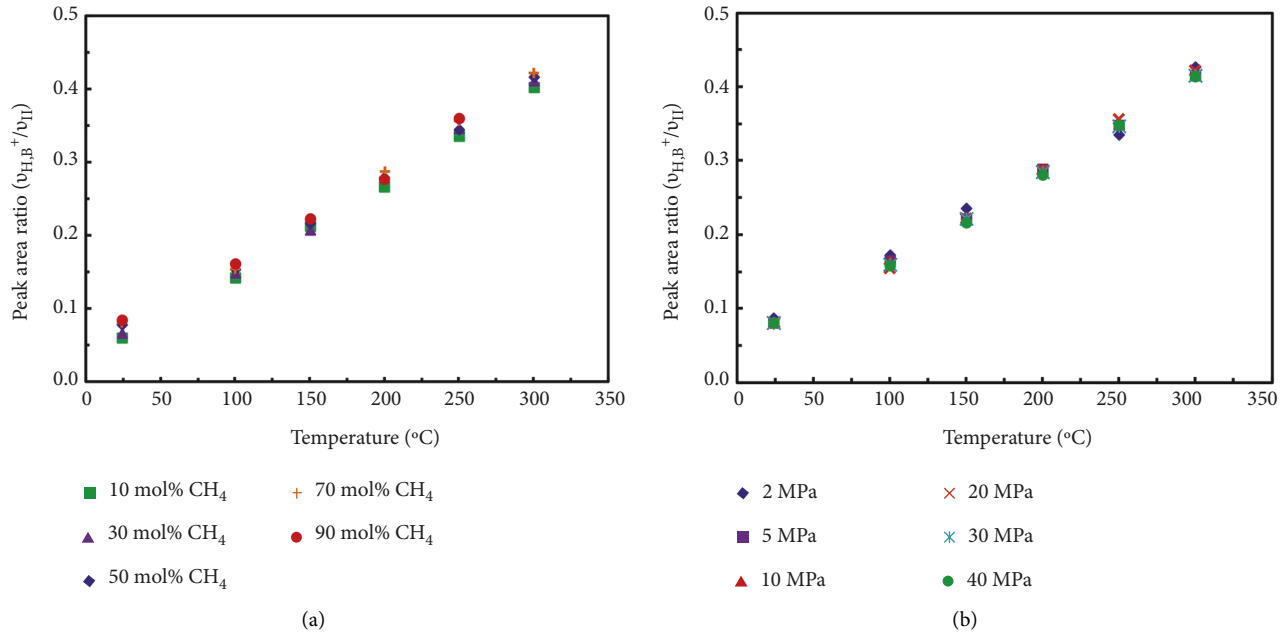

FIGURE 13: (a) Raman peak area ratio between the upper hot band and the upper Fermi domain versus temperature at 20 MPa for different CO_2-CH_4 mixtures. (b) Raman peak area ratio between the upper hot band and the upper Fermi domain versus temperature at 70% CH_4-30% CO_2 and different pressures.

temperature [37, 55, 56] and assessed the possibility of using the CO_2 hot band as a thermometer [57, 58]. In this study, we examined the relationship between the peak area ratio between the upper hot band ($\upsilon_{H,B}^{+}$) and the upper Fermi diad member (υ_{II}) with temperature, pressure, and composition. Figure 13 shows that the peak area ratio between the upper hot band and the upper Fermi domain is a sensitive function of temperature, and almost independent of composition and pressure. This indicates that the CO_2 hot band can be used as a thermometer in the CO_2-CH_4 gas mixtures.

5. Application to FSCC Samples

To verify the accuracy of the Raman quantitative analysis methods described above, six synthetic FIs in FSCC samples with unknown relative molar proportions of the components, total pressure, and density were prepared, and the results of microthermometric measurements for these samples were compared with laser Raman (LRM) spectroscopic data. Each FSCC sample was analyzed by MT to determine the melting temperature T_m and the homogenization temperature T_h, and they were used to calculate the composition and density of the fluid inclusion based on the VX diagram of Thiery et al. [18]. The total pressures were determined from MT using the GERG-2008 EoS. The selected FSCC samples were also analyzed three times with Raman spectroscopy. The average values of the CH_4 to CO_2 peak area ratio (A (CH_4)/A (CO_2)) and peak position of CH_4 (υ_{CH4}) were used to calculate the composition, pressure, and density through equations (1), (4), and (5). A comparison of the results obtained by LRM and MT is listed in Table 5 and plotted in Figure 14. The uncertainty for 1σ is also provided, and the procedure used for calculating the uncertainty propagation is the same as that reported by Le et al. [19].

For the LRM data, average errors in the values of mol% CH_4, pressure, and density, based on the differences between these three sets of analyses on the same FSCC samples and the best-fitted equations (1), (4), and (5), are ±1.2 mol%, ±0.9 MPa, and ±0.011 g·cm^{-3}, respectively. For the MT data, the uncertainty in ±0.1°C of the heating-cooling stage for T_m and T_h and an error in graphic reading arising from the VX diagram can result in average errors of ±1.0 mol% in composition and ±0.008 g/cm^3 in density, which can lead to an average error of ±1.1 MPa in pressure, as determined from the GERG-2008 EoS.

Overall, for the same FSCC samples, there is a very good agreement between the mol% CH_4 derived from LRM and MT analyses (Table 5, Figure 14(a)). The largest difference in mol% CH_4 is 2.1 mol%. The densities derived from LRM analysis are slightly smaller than those obtained from MT analysis, and the difference is within 0.062 g/cm^3 (Figure 14(c)). However, there is a large deviation between the pressure derived from LRM analysis and MT analysis (Figure 14(b)). To investigate the reason for the large deviation, the pressure (P_{cal1}) calculated from X_{Raman} and ρ_{Raman} and the density (ρ_{cal1}) calculated from X_{Raman} and P_{Raman} using the GERG-2008 EoS are also obtained (Table 5, Figures 14(b) and 14(c)), and they are very close to the values for P_{Raman} and ρ_{Raman} obtained directly using equations (4) and (5), respectively. The results show that our calibration equations could provide reasonable estimates for the composition, pressure, and density of fluid inclusions. Therefore, it is reasonable to believe that this deviation is derived from the deviation of density and composition between LRM analysis and MT analysis. Incredibly, the slight

Table 5: Comparison of the results obtained from Raman spectroscopy and microthermometry.

No.	Raman results[a]							Microthermometry results[b]					Difference[c]		
	A (CH_4)/A (CO_2)	υ_{CH4} (cm^{-1})	X_{Raman} mol% CH_4	P_{Raman} (MPa)	ρ_{Raman} ($g{\cdot}cm^{-3}$)	P_{cal1} (MPa)	ρ_{cal1} ($g{\cdot}cm^{-3}$)	T_m (°C)	T_h (°C)	$X_{Microth}$ mol% CH_4	$\rho_{Microth}$ ($g{\cdot}cm^{-3}$)	P_{cal2} (MPa)	ΔX mol%	ΔP (MPa)	$\Delta\rho$ ($g{\cdot}cm^{-3}$)
S.1	31.821 ±0.765	2911.342 ±0.006	86.6 ±0.1	50.2 ±0.8	0.345 ±0.003	48.8	0.349	−79.5	−89.1	87.5 ±0.8	0.364 ±0.005	59.6 ±1.1	−0.9	−9.4	−0.019
S.2	24.901 ±0.053	2911.644 ±0.029	83.1 ±0.5	42.2 ±1.2	0.342 ±0.006	41.3	0.345	−75.3	−83.1	82.5 ±1.2	0.398 ±0.006	61.1 ±0.8	0.6	−18.9	−0.056
S.3	12.214 ±0.487	2913.341 ±0.023	70.8 ±1.5	22.4 ±0.8	0.284 ±0.013	20.7	0.301	−67.4	−44.6	70.7 ±0.8	0.286 ±0.001	20.9 ±0.1	0.1	1.5	−0.002
S.4	4.907 ±0.036	2911.464 ±0.008	49.3 ±1.3	46.8 ±0.9	0.569 ±0.012	43.2	0.582	−65.6	−59.8	49.0 ±1.3	0.631 ±0.010	62.8 ±0.3	0.3	−16.0	−0.062
S.5	3.573 ±0.024	2911.469 ±0.008	41.4 ±1.9	46.7 ±0.8	0.636 ±0.017	44.8	0.643	−64.8	−64.2	43.5 ±1.1	0.677 ±0.012	64.3 ±3.0	−2.1	−17.6	−0.041
S.6	1.495 ±0.0011	2911.811 ±0.004	22.8 ±2.1	38.6 ±0.7	0.766 ±0.017	37.3	0.772	−61.7	−24.8	20.9 ±1.0	0.795 ±0.011	39.9 ±1.4	1.9	−1.3	−0.029

[a]X_{Raman}, $P_{Raman,}$ and ρ_{Raman} are determined from equations (1), (4), and (5) based on A (CH_4)/A (CO_2) and υ_{CH4}; P_{cal1} is the pressure calculated from X_{Raman} and ρ_{Raman} using the GERG-2008 EoS; ρ_{cal1} is the density calculated from X_{Raman} and P_{Raman} using the GERG-2008 EoS. [b]$X_{Microth}$ and $\rho_{Microth}$ are obtained from the VX diagram of Thiery et al. [18] based on T_m and T_h; P_{cal2} is the pressure calculated from $X_{Microth}$ and $\rho_{Microth}$ using the GERG-2008 EoS. [c]$\Delta X = X_{Raman} - X_{Microth}$. $\Delta P = P_{Raman} - P_{cal2}$. $\Delta\rho = \rho_{Raman} - \rho_{Microth}$. Note that all data are measured at room temperature (~24°C), and the uncertainty is provided for 1σ.

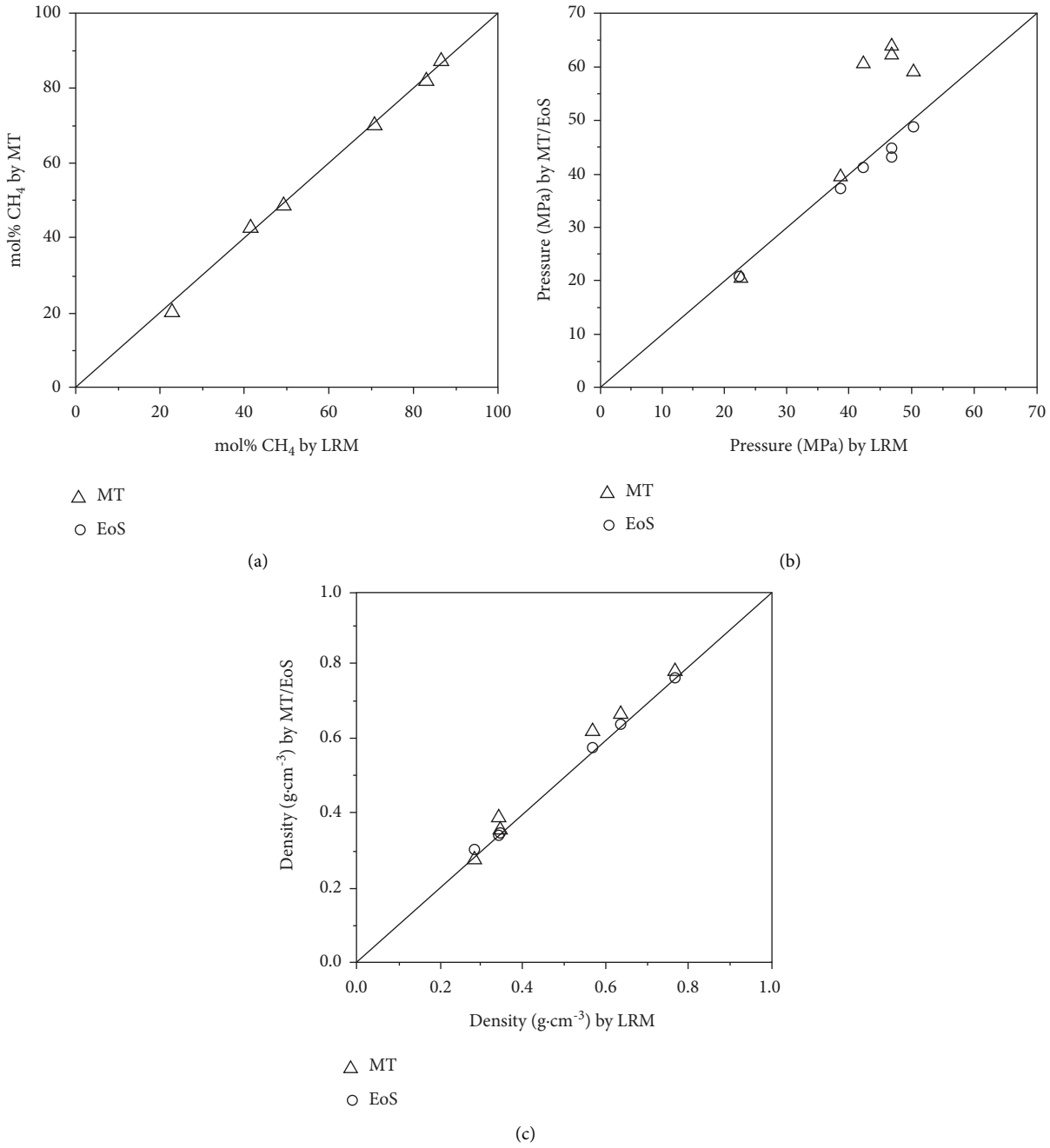

Figure 14: Comparison of (a) mol% CH_4, (b) pressure, and (c) density of CO_2-CH_4 mixtures in FSCCs based on laser Raman (LRM) and microthermometry (MT) data. Note that the pressure (b) and density (c) calculated by GERG-2008 EoS are based on X_{Raman} and ρ_{Raman}, and X_{Raman} and P_{Raman}, respectively.

deviation in density and composition can lead to such a large deviation in pressure. For example, a small difference between the composition of 0.6 mol% CH_4 and the density of 0.056 g/cm^3 can lead to a pressure deviation of up to 18.9 MPa (Table 5, Figure 14(b)). Although the uncertainty in the MT analysis is slightly better than that derived from the LRM analysis in this work, Raman spectroscopy is still a powerful tool for fluid inclusion investigations. In addition, for the analyses of natural fluid inclusions, MT may not be more efficient than LRM analysis in some cases, such as small inclusions (<5 μm) and inclusions with poor optical properties (color, contrast, etc.) or the formation of clathrates [20]. It is worth noting that when analyzing natural fluid inclusions in anisotropic host minerals by using Raman spectroscopy, it must be placed at crystal extinction position to eliminate the effect of birefringence of the host mineral on the composition of the gas phase of fluid inclusions, as suggested by Caumon et al. [59].

6. Conclusion

This study investigated the Raman spectral parameters (peak position and peak area) for CO_2-CH_4 mixtures at pressures up to 40 MPa and temperatures up to 300°C. The variation in each spectral parameter as a function of fluid pressure, density, temperature, and composition was discussed. The peak position of the v_1 band for CH_4 can be used to determine the pressure of pure CH_4 and CH_4-dominated fluids (>50 mol% CH_4). The relationships for the peak position of the v_1 band for CH_4, density, and composition were established and used to calculate the densities for CO_2-CH_4 mixtures. The Raman quantification factor $F(CH_4)/F(CO_2)$ was found to remain almost constant (5.048 ± 0.4) with varying pressure/density and composition, and, therefore, was used for the determination of the CH_4 to CO_2 molar ratio for fluids with high internal pressures (>10 MPa) based on the Raman peak area ratio. The effects of temperature on the variations in Raman spectral parameters were first investigated at temperatures up to 300°C, and these effects should not be ignored when Raman spectral parameters are used to calculate the pressure, density, and composition of CO_2-CH_4 gas mixtures. The results of our Raman spectroscopic measurements for six FSCC samples agree very well with those derived from MT analyses and, thus, verify our methodology for the quantitative determination of composition, pressure, and density of CO_2-CH_4 mixtures.

Data Availability

The data used to support the findings of this study are included within the supplementary materials.

Conflicts of Interest

The authors declare that there are no conflicts of interest.

Acknowledgments

This work was supported by the Key Frontier Science Program (QYZDY-SSW-DQC008) of the Chinese Academy of Sciences and the National Natural Science Foundation of China (Grants nos. 41973055 and 42130109). The authors thank Ms. Haiyan Zhang of the Institute of Deep-Sea Science and Engineering, Chinese Academy of Sciences, for her efforts in the purchase of experimental materials and Dr. Nanfei Cheng of the Institute of Deep-Sea Science and Engineering, Chinese Academy of Sciences, for English editing.

Supplementary Materials

Table S1. Calibrated Raman peak positions (cm^{-1}) of the CH_4v_1 peak for pure CH_4 gas and ten CO_2-CH_4 mixtures at room temperature (~24°C) and various pressures. The uncertainties were derived from the standard deviation of the three consecutive measurements of spectra at each *P-T* condition. Table S2. Calibrated Raman peak positions (cm^{-1}) of the lower and upper member of the CO_2 Fermi diad and the Fermi diad splits (Δ) of pure CO_2 gas and ten CO_2-CH_4 mixtures at room temperature (~24°C) and various pressures. The uncertainties were derived from the standard deviation of the three consecutive measurements of spectra at each *P-T* condition. Table S3. Calibrated Raman peak positions (cm^{-1}) of CH_4v_1 peak and Fermi diad splits (Δ) of CO_2 for pure CH_4 or CO_2 gas and their five CO_2-CH_4 mixtures at various temperatures and pressures. The uncertainties were derived from the standard deviation of the three consecutive measurements of spectra at each *P-T* condition. (*Supplementary Materials*)

References

[1] A. M. V. D. Kerkhof, *The system* CO_2-CH_4-N_2 *in fluid inclusions: ieoretical modeling and geological applications*, Ph.D. Dissertation, Free University of Amsterdam, Amsterdam, Netherlands, 1988.

[2] M. Cuney, Y. Coulibaly, and M. C. Boiron, "High-density early CO_2 fluids in the ultrahigh-pressure granulites of ihouhaouene (in Ouzzal, Algeria)," *Lithos*, vol. 96, no. 3-4, pp. 402–414, 2007.

[3] J. Yamamoto, H. Kagi, Y. Kawakami, N. Hirano, and M. Nakamura, "Paleo-moho depth determined from the pressure of CO_2 fluid inclusions: Raman spectroscopic barometry of mantle- and crust-derived rocks," *Earth and Planetary Science Letters*, vol. 253, no. 3-4, pp. 369–377, 2007.

[4] E. L. Klein and K. Fuzikawa, "Origin of the CO_2-only fluid inclusions in the palaeoproterozoic carará vein-quartz gold deposit, Ipitinga Auriferous district, SE-Guiana Shield, Brazil: implications for orogenic gold mineralization," *Ore Geology Reviews*, vol. 37, no. 1, pp. 31–40, 2010.

[5] J. Lai and G. Chi, "CO_2-rich fluid inclusions with chalcopyrite daughter mineral from the Fenghuangshan Cu-Fe-Au deposit, China: implications for metal transport in vapor," *Mineralium Deposita*, vol. 42, no. 3, pp. 293–299, 2007.

[6] H. R. Fan, F. F. Hu, K. Y. Wang, and Y. H. Xie, "Aqueous-carbonic-REE fluids in the giant Bayan Obo deposit, China: implications for REE mineralization," in *Mineral Deposit Research: Meeting the Global Challenge*, J. W. Mao and F. P. Bierlein, Eds., pp. 945–948, Springer, Beijing, China, 2005.

[7] J. Dubessy, S. Buschaert, W. Lamb, J. Pironon, and R. Thiery, "Methane-bearing aqueous fluid inclusions: Raman analysis, thermodynamic modelling and application to petroleum basins," *Chemical Geology*, vol. 173, no. 1–3, pp. 193–205, 2001.

[8] P. J. Wang, Q. J. Hou, K. Y. Wang, and S. M. Chen, "Discovery and significance of high CH_4 primary fluid inclusions in reservoir volcanic rocks of the Songliao basin, NE China," *Acta Geologica Sinica*, vol. 81, no. 1, pp. 113–120, 2007.

[9] J. Mullis, J. Dubessy, B. Poty, and J. O'Neil, "Fluid regimes during late stages of a continental collision: physical, chemical, and stable isotope measurements of fluid inclusions in fissure quartz from a geotraverse through the central Alps, Switzerland," *Geochimica et Cosmochimica Acta*, vol. 58, no. 10, pp. 2239–2267, 1994.

[10] D. S. Kelley, J. A. Karson, G. L. Früh-Green et al., "A serpentinite-hosted ecosystem: the lost city hydrothermal field," *Science*, vol. 307, no. 5714, pp. 1428–1434, 2005.

[11] D. S. Kelley and G. L. Früh-Green, "Abiogenic methane in deep-seated mid-ocean ridge environments: insights from stable isotope analyses," *Journal of Geophysical Research*, vol. 104, no. B5, pp. 10439–10460, 1999.

[12] M. Frey, M. Teichmuller, R. Teichmuller et al., "Very low-grade metamorphism in external parts of the central alps: illite crystallinity, coal rank and fluid inclusion data," *Eclogae Geologicae Helvetiae*, vol. 73, no. 1, pp. 173–203, 1980.

[13] B. Beeskow, A. H. Rankin, P. J. Murphy, and P. J. Treloar, "Mixed CH_4-CO_2 fluid inclusions in quartz from the south wales coalfield as suitable natural calibration standards for microthermometry and Raman spectroscopy," *Chemical Geology*, vol. 223, no. 1–3, pp. 3–15, 2005.

[14] W. T. Parry and N. J. F. Blamey, "Fault fluid composition from fluid inclusion measurements, Laramide age Uinta thrust fault, Utah," *Chemical Geology*, vol. 278, no. 1-2, pp. 105–119, 2010.

[15] J. C. Seitz, J. D. Pasteris, and G. B. Morgan, "Quantitative analysis of mixed volatile fluids by Raman microprobe spectroscopy: a cautionary note on spectral resolution and peak shape," *Applied Spectroscopy*, vol. 47, no. 6, pp. 816–820, 1993.

[16] J. C. Seitz, J. D. Pasteris, and I. M. Chou, "Raman spectroscopic characterization of gas mixtures. I. Quantitative composition and density determination of CH_4, N_2, and their mixtures," *American Journal of Science*, vol. 293, no. 4, pp. 297–321, 1993.

[17] J. C. Seitz, J. D. Pasteris, and I. M. Chou, "Raman spectroscopic characterization of gas mixtures; II, quantitative composition and pressure determination of the CO_2-CH_4 system," *American Journal of Science*, vol. 296, no. 6, pp. 577–600, 1996.

[18] R. Thiery, A. M. V. D. Kerkhof, and J. Dubessy, "VX properties of CH_4-CO_2 and CO_2-N_2 fluid inclusions: modelling for $T < 31^oC$ and $P < 400$ bars," *European Journal of Mineralogy*, vol. 6, no. 6, pp. 753–771, 1994.

[19] V. H. Le, M. C. Caumon, A. Tarantola, A. Randi, P. Robert, and J. Mullis, "Quantitative measurements of composition, pressure, and density of microvolumes of CO_2-N_2 gas mixtures by Raman spectroscopy," *Analytical Chemistry*, vol. 91, no. 22, pp. 14359–14367, 2019.

[20] V. H. Le, M. C. Caumon, A. Tarantola, A. Randi, P. Robert, and J. Mullis, "Calibration data for simultaneous determination of P-V-X properties of binary and ternary CO_2-CH_4-N_2 gas mixtures by Raman spectroscopy over 5–600 bar: application to natural fluid inclusions," *Chemical Geology*, vol. 552, Article ID 119783, 2020.

[21] D. Guillaume, S. Teinturier, J. Dubessy, and J. Pironon, "Calibration of methane analysis by Raman spectroscopy in H_2O-NaCl-CH_4 fluid inclusions," *Chemical Geology*, vol. 194, no. 1–3, pp. 41–49, 2003.

[22] W. Ou, L. Geng, W. Lu, H. Guo, K. Qu, and P. Mao, "Quantitative Raman spectroscopic investigation of geo-fluids high-pressure phase equilibria: Part II. Accurate determination of CH_4 solubility in water from 273 to 603 K and from 5 to 140 MPa and refining the parameters of the thermodynamic model," *Fluid Phase Equilibria*, vol. 391, pp. 18–30, 2015.

[23] H. Guo, Y. Chen, Q. Hu, W. Lu, W. Ou, and L. Geng, "Quantitative Raman spectroscopic investigation of geo-fluids high-pressure phase equilibria: Part I. Accurate calibration and determination of CO_2 solubility in water from 273.15 to 573.15 K and from 10 to 120 MPa," *Fluid Phase Equilibria*, vol. 382, pp. 70–79, 2014.

[24] M. C. Caumon, P. Robert, E. Laverret et al., "Determination of methane content in NaCl-H_2O fluid inclusions by Raman spectroscopy. Calibration and application to the external part of the central Alps (Switzerland)," *Chemical Geology*, vol. 378-379, pp. 52–61, 2014.

[25] M. C. Caumon, J. Dubessy, P. Robert, and B. Benaissa, "Microreactors to measure solubilities in the CO_2-H_2O-NaCl system," *Energy Procedia*, vol. 114, pp. 4843–4850, 2017.

[26] I. M. Chou, J. D. Pasteris, and J. C. Seitz, "High-density volatiles in the system C-O-H-N for the calibration of a laser Raman microprobe," *Geochimica et Cosmochimica Acta*, vol. 54, no. 3, pp. 535–543, 1990.

[27] V. Thieu, S. Subramanian, S. O. Colgate, and E. D. Sloan Jr., "High-pressure optical cell for hydrate measurements using Raman spectroscopy," *Annals of the New York Academy of Sciences*, vol. 912, no. 1, pp. 983–992, 2000.

[28] F. Lin, R. J. Bodnar, and S. P. Becker, "Experimental determination of the Raman CH_4 symmetric stretching (v_1) band position from 1 to 650 bar and 0.3–22°C: application to fluid inclusion studies," *Geochimica et Cosmochimica Acta*, vol. 71, no. 15, pp. 3746–3756, 2007.

[29] W. Lu, I. M. Chou, R. C. Burruss, and Y. Song, "A unified equation for calculating methane vapor pressures in the CH_4-H_2O system with measured Raman shifts," *Geochimica et Cosmochimica Acta*, vol. 71, no. 16, pp. 3969–3978, 2007.

[30] L. B. Shang, I. M. Chou, R. C. Burruss, R. Z. Hu, and X. Bi, "Raman spectroscopic characterization of CH_4 density over a wide range of temperature and pressure," *Journal of Raman Spectroscopy*, vol. 45, no. 8, pp. 696–702, 2014.

[31] J. Zhang, S. Qiao, W. Lu, Q. Hu, S. Chen, and Y. Liu, "An equation for determining methane densities in fluid inclusions with Raman shifts," *Journal of Geochemical Exploration*, vol. 171, pp. 20–28, 2016.

[32] Y. Qiu, X. L. Wang, X. Liu et al., "In situ Raman spectroscopic quantification of CH_4-CO_2 mixture: application to fluid inclusions hosted in quartz veins from the longmaxi formation shales in Sichuan Basin, southwestern China," *Petroleum Science*, vol. 17, no. 1, pp. 23–35, 2020.

[33] D. M. Sublett, E. Sendula, H. Lamadrid et al., "Shift in the Raman symmetric stretching band of N_2, CO_2, and CH_4 as a function of temperature, pressure, and density," *Journal of Raman Spectroscopy*, vol. 51, no. 3, pp. 555–568, 2020.

[34] Y. Kawakami, J. Yamamoto, and H. Kagi, "Micro-Raman densimeter for CO_2 inclusions in mantle-derived minerals," *Applied Spectroscopy*, vol. 57, no. 11, pp. 1333–1339, 2003.

[35] J. Yamamoto and H. Kagi, "Extended micro-Raman densimeter for CO_2 applicable to mantle-originated fluid inclusions," *Chemistry Letters*, vol. 35, no. 6, pp. 610-611, 2006.

[36] Y. Song, I. Chou, W. Hu, B. Robert, and W. Lu, "CO_2 density-Raman shift relation derived from synthetic inclusions in fused silica capillaries and its application," *Acta Geologica Sinica-English Edition*, vol. 83, no. 5, pp. 932–938, 2009.

[37] X. Wang, I. M. Chou, W. Hu, R. C. Burruss, Q. Sun, and Y. Song, "Raman spectroscopic measurements of CO_2 density: experimental calibration with high-pressure optical cell (HPOC) and fused silica capillary capsule (FSCC) with application to fluid inclusion observations," *Geochimica et Cosmochimica Acta*, vol. 75, no. 14, pp. 4080–4093, 2011.

[38] M. L. Frezzotti, F. Tecce, and A. Casagli, "Raman spectroscopy for fluid inclusion analysis," *Journal of Geochemical Exploration*, vol. 112, pp. 1–20, 2012.

[39] H. M. Lamadrid, L. R. Moore, D. Moncada, J. D. Rimstidt, R. Burruss, and R. Bodnar, "Reassessment of the Raman CO_2 densimeter," *Chemical Geology*, vol. 450, pp. 210–222, 2017.

[40] W. Wang, M. C. Caumon, A. Tarantola, J. Pironon, W. Lu, and Y. Huang, "Raman spectroscopic densimeter for pure

CO_2 and CO_2-H_2O-NaCl fluid systems over a wide P-T range up to 360°C and 50 MPa," *Chemical Geology*, vol. 528, Article ID 119281, 2019.

[41] Y. Hagiwara, J. Torimoto, and J. Yamamoto, "Pressure measurement and detection of small H_2O amounts in high-pressure H_2O-CO_2 fluid up to 141 MPa using fermi diad splits and bandwidths of CO_2," *Journal of Raman Spectroscopy*, vol. 51, no. 6, pp. 1003–1018, 2020.

[42] Y. Hagiwara, T. Kawano, K. Takahata, J. Torimoto, and J. Yamamoto, "Temperature dependence of a Raman CO_2 densimeter from 23°C to 200°C and 7.2 to 248.7 MPa: evaluation of density underestimation by laser heating," *Journal of Raman Spectroscopy*, vol. 52, no. 10, pp. 1744–1757, 2021.

[43] D. M. Sublett, E. Sendula, H. M. Lamadrid, M. Steele-MacInnis, G. Spiekermann, and R. J. Bodnar, "Raman spectral behavior of N_2, CO_2, and CH_4 in N_2-CO_2-CH_4 gas mixtures from 22°C to 200°C and 10 to 500 bars, with application to other gas mixtures," *Journal of Raman Spectroscopy*, vol. 52, no. 3, pp. 750–769, 2021.

[44] B. Wopenka and J. D. Pasteris, "Raman intensities and detection limits of geochemically relevant gas mixtures for a laser Raman microprobe," *Analytical Chemistry*, vol. 59, no. 17, pp. 2165–2170, 1987.

[45] H. W. Schrötter and H. W. Klöckner, *Raman Spectroscopy of Gases and Liquids*, A. Weber, Ed., vol. 11, Springer, Berlin, Germany, 1979.

[46] E. A. J. Burke, "Raman microspectrometry of fluid inclusions," *Lithos*, vol. 55, no. 1–4, pp. 139–158, 2001.

[47] I. M. Chou, Y. Song, and R. C. Burruss, "A new method for synthesizing fluid inclusions in fused silica capillaries containing organic and inorganic material," *Geochimica et Cosmochimica Acta*, vol. 72, no. 21, pp. 5217–5231, 2008.

[48] L. Jiang, Y. Xin, I. M. Chou, and Y. Chen, "Raman spectroscopic measurements of ν_1 band of hydrogen sulfide over a wide range of temperature and density in fused-silica optical cells," *Journal of Raman Spectroscopy*, vol. 49, no. 2, pp. 343–350, 2018.

[49] S. Mao, L. Shi, Q. Peng, and M. Lu, "Thermodynamic modeling of binary CH_4-CO_2 fluid inclusions," *Applied Geochemistry*, vol. 66, pp. 65–72, 2016.

[50] M. Wang, W. Lu, L. Li, and S. Qiao, "Pressure and temperature dependence of the Raman peak intensity ratio of asymmetric stretching vibration ($v3$) and asymmetric bending overtone ($2v2$) of methane," *Applied Spectroscopy*, vol. 68, no. 5, pp. 536–540, 2014.

[51] S. B. Hansen, R. W. Berg, and E. H. Stenby, "Raman spectroscopic studies of methane-ethane mixtures as a function of pressure," *Applied Spectroscopy*, vol. 55, no. 6, pp. 745–749, 2001.

[52] F. Varzandeh, E. H. Stenby, and W. Yan, "Comparison of GERG-2008 and simpler EoS models in calculation of phase equilibrium and physical properties of natural gas related systems," *Fluid Phase Equilibria*, vol. 434, pp. 21–43, 2017.

[53] J. Dubessy, B. Poty, and C. Ramboz, "Advances in C-O-H-N-S fluid geochemistry based on micro-Raman spectrometric analysis of fluid inclusions," *European Journal of Mineralogy*, vol. 1, no. 4, pp. 517–534, 1989.

[54] B. Xi, W. Shi, H. Jiang, and Y. Qian, "Synthesis of N_2-CH_4 and N_2-CO_2 gas mixtures as an online standard and determination of their Raman quantification factors of CH_4 and CO_2," *Rock and Mineral Analysis*, vol. 33, no. 5, pp. 655–660, 2014, in Chinese.

[55] M. Arakawa, J. Yamamoto, and H. Kagi, "Micro-Raman thermometer for CO_2 fluids: temperature and density dependence on Raman spectra of CO_2 fluids," *Chemistry Letters*, vol. 37, no. 3, pp. 280-281, 2008.

[56] Y. Hagiwara, K. Takahata, J. Torimoto, and J. Y Amamoto, "CO_2 Raman thermometer improvement: comparing hot band and stokes and anti-stokes Raman scattering thermometers," *Journal of Raman Spectroscopy*, vol. 49, no. 11, pp. 1776–1781, 2018.

[57] M. S. Brown and R. R. Steeper, "CO_2-based thermometry of supercritical water oxidation," *Applied Spectroscopy*, vol. 45, no. 10, pp. 1733–1738, 1991.

[58] Y. Hagiwara, K. Yoshida, A. Yoneda, J. Torimoto, and J. Yamamoto, "Experimental variable effects on laser heating of inclusions during Raman spectroscopic analysis," *Chemical Geology*, vol. 559, Article ID 119928, 2021.

[59] M. Caumon, A. Tarantola, and W. Wang, "Raman spectra of gas mixtures in fluid inclusions: effect of quartz birefringence on composition measurement," *Journal of Raman Spectroscopy*, vol. 51, no. 9, pp. 1868–1873, 2019.